Turbulence, Heat and Mass Transfer 6
K. Hanjalić, Y. Nagano and S. Jakirlić (Editors)

Filtered simulation method for turbulent heat and mass transfer in gas dynamic flows

T.G. Elizarova[1] and V.V. Seregin[2]

[1]*Institute for Mathematical Modeling, Russian Academy of Sciences, Miusskaya pl. 4a, Moscow, 125047, Russia, telizar@yahoo.com*

[2]*Departement of Mathematics, Faculty of Physics, Moscow State University, Leninskie gory, Moscow, 119992 Russia, v.seregin@gmail.com*

Abstract — The novel mathematical model for unified simulation both laminar and low-Reynolds turbulent flow, including the bifurcation point, is described and tested. This model is based on the quasi-gas dynamic equations, that differ from the Navier-Stokes system by the additional nonlinear dissipative terms. In turbulent flow simulations these additional terms play the role of subgrid dissipation. The results of simulations for a backward-facing step flow in 2D and 3D configurations are presented.

1. Introduction

LES models play an increasing role in numerical simulation of turbulent heat and mass transfer for engineering applications. Here the quality of the numerical solution depends strongly on the properties of the filter-type model, that is used to reproduce subgrid-type dissipation. The most popular and robust model seems to be the Smagorinsky model [1] and its variations. In this model the filter size is determined by the space step of the computational grid. The eddy viscosity is assumed to be proportional to the subgrid-scale characteristic length, that plays the role of the filter. Turbulent dissipative terms have the traditional mathematical form, similar to the Navier-Stokes dissipative terms. However, this model cannot be considered as perfect. Particulary, close to a wall the model is too dissipative, which produces difficulties in modeling laminar-turbulent transition. Also the determination of the characteristic constants, needed by the model, is not well-established.

In the present paper we describe a novel mathematical model, that can be regarded as a nice alternative to existing filter models for LES methods and can be used for unified simulations of both laminar and low-Reynolds turbulent flows. This model is based on the quasi-gas dynamic (QGD) equation system, that generalizes the Navier-Stokes (NS) system and differs from it by additional nonlinear dissipative terms. These terms include a multiplicative parameter τ which has the dimension of a time. The additional dissipation appears in all gas dynamic equations in the form of strongly non-linear τ-terms. The influence of additional terms is inessential for the stationary flows of non-rarefied gases. But for strongly nonstationary flows and also for moderately rarefied flows their contribution becomes essential, and in these classes the advantages of QGD models were seen. In the numerical modeling the τ-terms manifest themselves as effective regularizers, and corresponding numerical methods were tested for a number of heat and mass transfer problems of laminar viscous gas flows, e.g. [2], [3], [4] and citations therein.

The first backward-facing step flow simulations in 2D configuration show, that τ-terms provide the unified simulation of both laminar and low-Reynolds turbulent flows, including the bifurcation point. Particulary, these terms stabilize the numerical solution in laminar flow, and

play the role of subgrid dissipation for strongly nonstationary turbulent flow regime [5], [6]. In the present paper this result is verified in 3D calculations.

2. Quasi-gasdynamic model

The physical background for the QGD equation system is based on a time-averaging technique involving a small control volume, taking into account a corresponding small time interval. The QGD system generalizes the NS system of equations but differs from the NS system by additional dissipative terms with a small multiplicative parameter τ (e.g. [2] – [4] and citations included). The QGD system has a form of conservation laws, and in the absence of external forces in common notations writes as

$$\frac{\partial}{\partial t}\,\rho + \frac{\partial}{\partial x_i}\,j_{mi} = 0, \tag{1}$$

$$\frac{\partial}{\partial t}\,\rho u_i + \frac{\partial}{\partial x_j}\,j_{mj}u_i + \frac{\partial}{\partial x_i}\,p = \frac{\partial}{\partial x_j}\,\Pi_{ji}, \tag{2}$$

$$\frac{\partial}{\partial t}\,\rho\left(\frac{u^2}{2}+\varepsilon\right) + \frac{\partial}{\partial x_i}\,j_{mi}\left(\frac{u^2}{2}+\varepsilon+\frac{p}{\rho}\right) + \frac{\partial}{\partial x_i}\,q_i = \frac{\partial}{\partial x_i}\,\Pi_{ij}u_j. \tag{3}$$

The mass flow density vector j_m, viscous stress tensor Π, and heat flux q are given by

$$j_{mi} = \rho(u_i - w_i), \qquad w_i = \frac{\tau}{\rho}\left(\frac{\partial}{\partial x_j}\,\rho u_i u_j + \frac{\partial}{\partial x_i}\,p\right), \tag{4}$$

$$\Pi_{ij} = \Pi_{\mathrm{NS_{ij}}} + \tau\rho u_i\left(u_k\,\frac{\partial}{\partial x_k}\,u_j + \frac{1}{\rho}\,\frac{\partial}{\partial x_j}\,p\right) + \tau\delta_{ij}\left(u_k\,\frac{\partial}{\partial x_k}\,p + \gamma p\,\frac{\partial}{\partial x_k}\,u_k\right), \tag{5}$$

$$q_i = q_{\mathrm{NS\,i}} - \tau\rho u_i\left(u_j\,\frac{\partial}{\partial x_j}\,\varepsilon + pu_j\,\frac{\partial}{\partial x_j}\,\frac{1}{\rho}\right). \tag{6}$$

where Π_{NS} and q_{NSi} are the NS viscous stress tensor and heat flux vector, respectively. Eqs.4 - 6 show the additional τ-terms, included in vectors of mass flux, heat flux and viscous stress tensor.

The system (1) – (6) is completed by the state equation for a perfect gas, and with expressions for the coefficients of viscosity, heat conductivity and parameter τ. Heat conductivity coefficient æ and parameter τ are related through the viscosity coefficient μ by:

$$æ = \frac{\gamma\mathcal{R}}{(\gamma-1)Pr}\,\mu, \quad \tau = \frac{\mu}{p\,Sc}\,, \quad \mu = \mu_0\Big(\frac{T}{T_0}\Big)^{\omega}, \tag{7}$$

where Pr is the Prandtl number, Sc is the Schmidt number, $\mathcal{R}$ is the perfect-gas constant, and γ is the specific heat ratio. We use the power law $\mu = \mu_0(T/T_0)^{\omega}$ for the viscosity thermal dependence.

The entropy production X for the QGD system is the entropy production for the NS system completed by the additional terms in τ, that are the squared left-hand sides of the classical stationary Euler equations with positive coefficients:

$$X = æ\Big(\frac{\vec{\nabla}T}{T}\Big)^2 + \frac{(\Pi_{NS}:\Pi_{NS})}{2\eta T} + \frac{p\tau}{\rho^2 T}\Big[div(\rho\vec{u})\Big]^2 +$$
$$+\frac{\tau}{\rho T}\Big[\rho(\vec{u}\cdot\vec{\nabla})\vec{u} + \vec{\nabla}p\Big]^2 + \frac{\tau}{\rho\varepsilon T}\Big[\rho(\vec{u}\cdot\vec{\nabla})\varepsilon + pdiv\vec{u}\Big]^2.$$

Above equation proves the dissipative nature of the additional τ-terms and the correctness of the QGD model with respect to the second law of thermodynamic.

In the limit $\tau \to 0$, the QGD system reduces to the classical NS system. The QGD system differs from the NS one by second order space derivative terms of order $O(\tau)$, but for stationary flows, the dissipative terms (terms in τ) have the asymptotic order of $O(\tau^2)$ for $\tau \to 0$. In the boundary layer limit, terms in τ vanish, and both QGD and NS equation systems reduce to Prandtl's system. The entropy theorem for QGD system confirms the dissipative nature of τ-regularizers.

The continuity equation (1) of the QGD system involves the spatial derivative of the pressure, which makes it a second-order equation in space. Therefore, when standing the boundary conditions, an additional as compared with the NS system boundary condition is required. This condition is obtained directly from the condition for the mass flux density j_m (4) and the desired velocity conditions on the boundaries. For example, in the problem below this additional condition has the form of the pressure condition $\partial p/\partial n = 0$, where n is the normal to the boundary. Initial conditions for the QGD system are the same as for the NS one.

In calculations parameter τ is defined as

$$\tau = \frac{\mu}{p\, Sc} + \alpha \frac{h}{c}\,, \tag{8}$$

where h is the width of the grid filter (the mesh size in numerical computations), $c = \sqrt{\gamma RT}$ is the local speed of sound, $0 \le \alpha \le 1$ is a numerical coefficient to be determined, and h/c is the time required for a perturbation to travel across a grid cell. In modeling rarefied flows $\alpha = 0$, for other cases $\alpha \sim 0.5$. Depending of the problem, τ-value may be estimated otherwise, for example in atmospheric turbulent flows incorporating the experimental data for the macrodiffusion coefficients.

In the last years a number of new gasdynamic models with nonclassical continuity equation, namely the dissipative continuity equations, or so called two-velocity modes, were proposed by, e.g., [7] – [11]. The possibilities of these models for turbulent flow simulations were widely discussed, but newer verified in any practical calculations. Mention, that all these models differ from the present QGD equation system, that can be regarded as the system of the same family. Models [7]-[10] do not include the velocity derivatives in mass flux vector. The system [11] includes the second time derivatives, that do not appeared in the QGD model.

3. Problem formulation and numerical implementation

The test problem considered here is a subsonic airflow behind a backward facing step, e.g. [12, 13, 14] and citations included. The results of the QGD simulations in 2D formulation are reported in [5] and [6]. Here the QGD results are completed and proved by 3D computations.

The results for 3D numerical calculations for Mach number $Ma = 0.1, Re = 3500$ for the air flow with

$$\gamma = 1.4, Pr = 0.737, Sc = 0.746, \omega = 0.74,$$

are presented below. In cartesian coordinates computational domain (see Figs. 3 - 4) has the dimensions $L_x = 16, L_y = L_z = 2$, with backward-step dimensions $H_x = H_z = 1, H_y = 2$. We used the uniform space grids to resolve the vortex structures properely. The Reynolds and Mach numbers are defined as

$$Re = \frac{\rho_0 U_0 H_z}{\mu_0}, \qquad Ma = \frac{U_0}{c_0}, \tag{9}$$

with density ρ_0 and temperature T_0 at inlet, where the mean entrance velocity is

$$U_0 = \int u_x dy.$$

Boundary conditions are the following: left entrance boundary

$$u_x = 6(2-z)(1-z), \quad u_y = u_z = 0, \quad \frac{\partial p}{\partial x} = -12/Re,$$

right exit boundary

$$\frac{\partial f}{\partial x} = 0, \quad f = (\rho, u_x, u_y, u_z), \quad p = \frac{1}{\gamma M a^2},$$

step surfaces and lower plane

$$\frac{\partial \rho}{\partial n} = 0, \quad \frac{\partial p}{\partial n} = 0, \quad u_x = u_y = u_z = 0,$$

other boundaries

$$\frac{\partial f}{\partial n} = 0, \quad f = (\rho, p, u_s), \quad u_n = 0,$$

where n is a normal vector to the boundary, s is a tangential vector.

For QGD calculations the explicit in time finite-volume method with central difference approximation for all space derivatives is used, where τ terms provide the stability of the numerical solution.

For 3D flows several improvements reducing computing time were made for the current software implementation. Firstly, entire necessary partial derivatives are computed by one time for each node of the finite-difference scheme due to utilizing of these derivaties in the conservation laws for gas-dynamics parameters namely density, velocity and pressure, in the same manner. Secondly, gas-dynamics values at half-integer mesh nodes are computed once per time step.

4. Computational results

Figs.1 consequently shows the temporal evolution of the velocity for laminar (Re=300), transitional (Re=600) and low-Reynolds turbulent (Re=3500) regimes in 2D calculations.

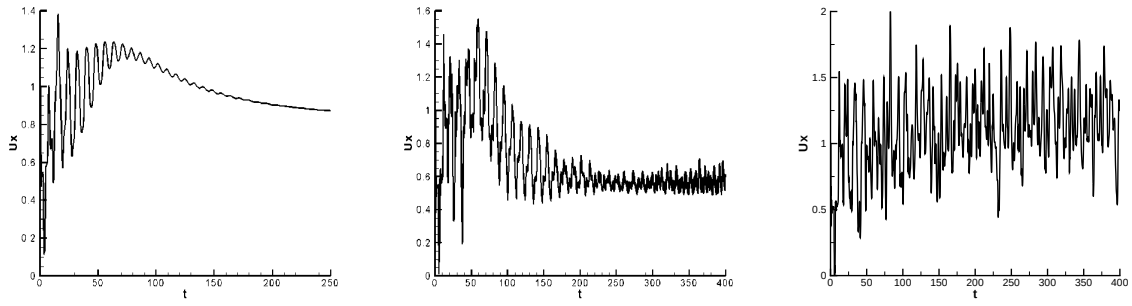

Figure 1: Time-evolution of u_x at $Re = 300$, 600 and 3500. 2D calculations

The normalized lengths L_s of the separation zones calculated for α = 0.5 and 0.3 are shown in fig.2, 2D results. Both solutions are mutually consistent and are consistent with the experiments for laminar flows, $Re < 600$. The solutions also agrees with experiment for turbulent flows,

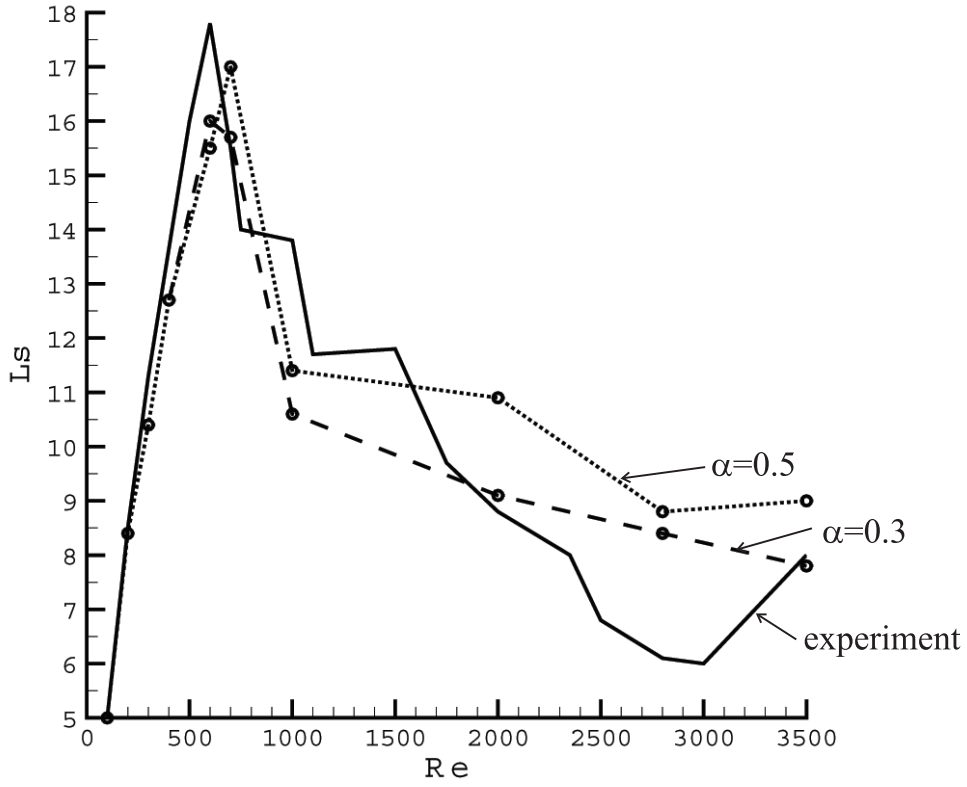

Figure 2: Separation zone length. Dash-lines - calculations [5], the full line - data [12].

$Re > 800$. The calculated Re values for the transition point slightly depend on the mesh step h ($h = 0.075, 0.05$ and 0.03) and τ values, but nevertheless qualitatively correspond to the experimental predictions of Armaly et al [12].

The uniform numerical method with only one free parameter τ is used for both laminar and turbulent regimes. Calculations for laminar flows show that factor α acts only on the stability of the QGD algorithm: with $\alpha \to 0$, the numerical time step must tend to zero to ensure stability of the method. However the solution does not depend on α. On the contrary, for strongly non-stationary turbulent flows, the numerical solution slightly depends on α (Fig. 2). Both solutions are mutually consistent and are consistent with experiment for laminar flows with $Re < 600$. The solutions also agrees with experiment for turbulent flows with $Re > 800$. Details of 2D calculations are presented in [5]. Equation system and numerical results for incompressible flows in comparison with PIV measurement are reported in [4], [15].

The validity of 2D calculations were proved by 3D calculations, that were performed for Re=3500 for $\alpha = 0.5$ in (8) and grid steps $h = 0.2, 0.1$ and 0.05 with non-dimensional time-steps equal to $\Delta t = 0.005, 0.0025$ and 0.001, respectively.

In a coarse grid $h = 0.2$ the subgrid dissipation proportional to $\tau \sim h$ suppresses the oscillations and the flow evolutes to a stationary picture. The grid steps $h = 0.1$ and 0.05 allow to obtain the nonstationary regime. In Figs. 3 the examples of instantaneous stream functions for developed flow are shown. Fig. 4 presents the 3D time-averaged flowfield ($h = 0.1$).

The stream-functions in symmetry plane for the time-averaged flow is shown in Figs. 5 for space steps $h = 0.1$ and 0.05 (left). For comparison the similar results for 2D calculations are shown in the same figure (right), both obtained for $\alpha = 0.5$. It demonstrates that for

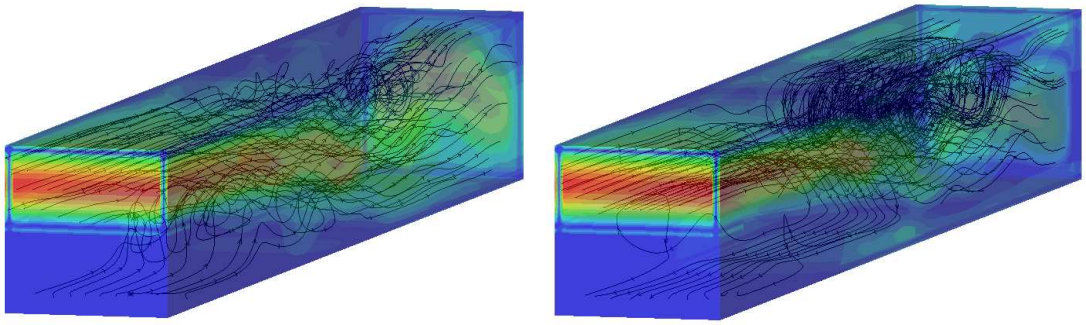

Figure 3: Instantaneous 3D stream functions in backward-facing step flow, fragments corresponding to different times t.

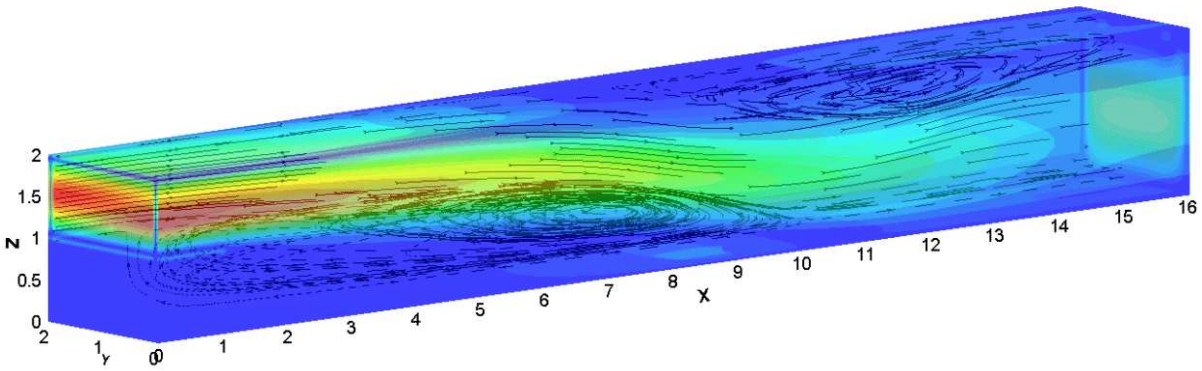

Figure 4: Averaged 3D stream functions in backward-facing step flow.

the symmetry plane the time-averaged 2D and 3D calculations give the similar results. When decreasing the space step more fine details of the flow structure are resolved – for the finer grids the additional inner vortex structures behind the step are seen in 2D and 3D formulations.

Figs. 6 show the sequence of the slides with stream-functions for the time-averaged flow in the sections $x = 3, 5, 5, 9, 11, 12.5$ and 13, for $h = 0.1$. The symmetry of the flow field related to a plane $y = 1$ is seen. Newetheless, the instantaneous 3D flowfields are non-symmetrical, see Figs. 3.

Fig. 7 presents the onset and the evolution of u_y in the symmetry plane for x = 5, 10 and 15. It is seen the development of the fluctuations of the transversal velocity with increasing of the time and the distance from the step. Here the onset of the fluctuations starts at $t \sim 1500$.

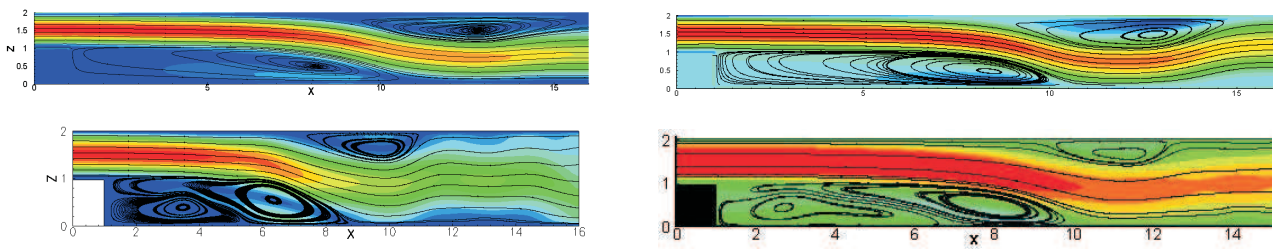

Figure 5: Left: 3D calculations, $h = 0.1$ (up) and 0.05 (down). Right: 2D calculations, $h = 0.1$ (up) and 0.05 (down)

In calculations with smaller grid step ($h = 0.05$) the transversal oscillations arise earlier, at $t \sim 200$.

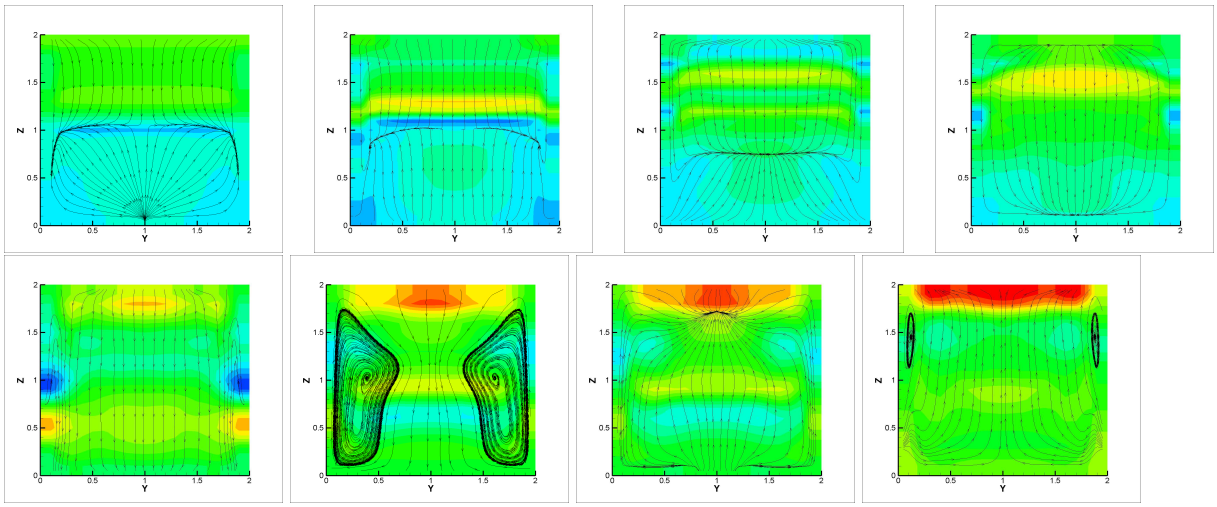

Figure 6: Slides for x=3, 5, 7, 9, 11, 12.5, 13 and 15.

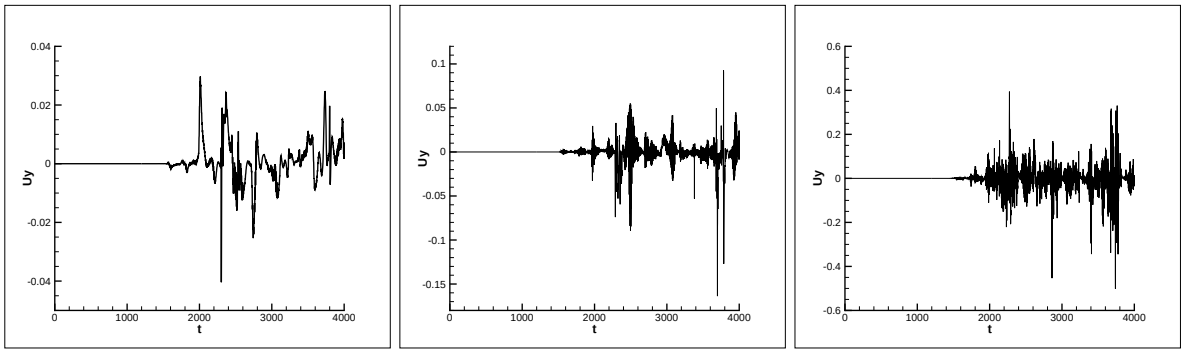

Figure 7: Time-evolution for u_y in the symmetry plane for x=5, 10 and 15, z=0.5.

The time evolutions for velocity components u_x, u_y and u_z in the point placed behind the step with coordinates (2.5,0.5,0.5) are plotted in Figs. 8 for $h = 0.1$ calculations. The fragments of the evolutions for u_x and u_y are seen in Fig. 9. Compared with 2D case (Fig. 1) one can see the additional low-frequency oscillations related with the third dimension of the computational domain.

Figs.10 presents spectra for u_x and u_z velocity components. According to these figures the main Strouhal frequencies obtained here are $f_1 \sim 0.1644$, corresponding to a time-period $\Delta t \sim 6$, and $f_2 \sim 0.004$ $(\Delta t \sim 250)$. f_1 value is close to the main frequency in 2D flow ([5] and [6]) and last picture in Fig.1), while the f_2 value is related with the third H_y dimension of the channel that is taken into consideration in the present calculations.

5. Conclusions

The obtained results for 2D and 3D backward-facing step flow show the possibilities of the QGD model as a filtered method for numerical simulation of turbulent heat and mass transfer in gasdynamic flows including the transition regime. This new filtered method must be tested

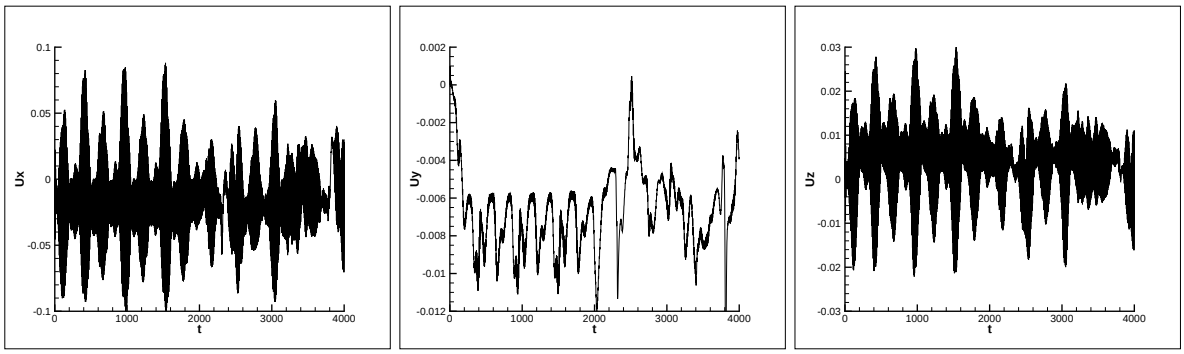

Figure 8: Time-evolution for u_x, u_y and u_z.

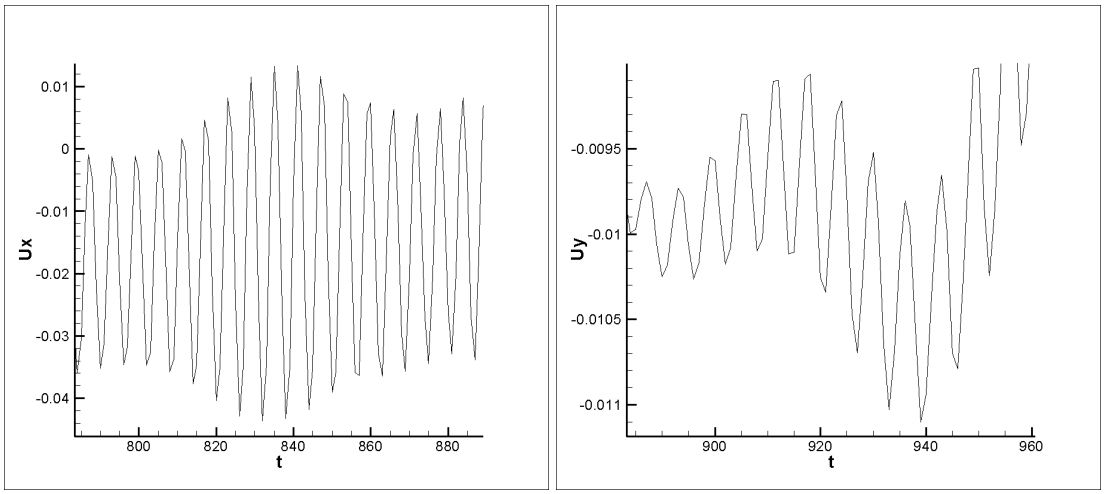

Figure 9: Fragments of time-evolution for u_x and u_y.

for other gas dynamic turbulent flows in order to clarify the domain of validity and the values of regularization parameter for practical simulations.

References

1. M. Lesieur. Turbulence in fluids. Springer, 2008.
2. T.G. Elizarova. Quasi-gasdynamic equations and numerical methods for viscous flow simulations. Moscow, Scientific world, 2007 (in Russian). English translation by Springer, 2009.
3. T.G. Elizarova, A.A. Khokhlov, Yu.V. Sheretov. Quasi-gasdynamic numerical algorithm for gas flow simulations. *Int.J. Numer. Meth. Fluids*, 56, No 8, 1209-1215, 2008.
4. Yu.V. Sheretov. Dynamics of continuum media in space-temporal averaging. Moscow, Izhevsk, 2009 (in Russian). http://ics.org.ru
5. T.G. Elizarova, P.N. Nikol'skii. Numerical simulation of the laminar-turbulent transition in the flow over a backward-facing step. *Moscow University Physics Bulletin*, 62, No4, 216-220, 2007.
6. T.G. Elizarova, P.N. Nikolskii, J.C. Lengrand. A new variant of subgrid dissipation for LES methods and simulation of laminar-turbulent transition in subsonic gas flows. *Notes on numerical fluid mechanics and multidisciplinary design*. 97, pp.289-298, Springer, 2008.

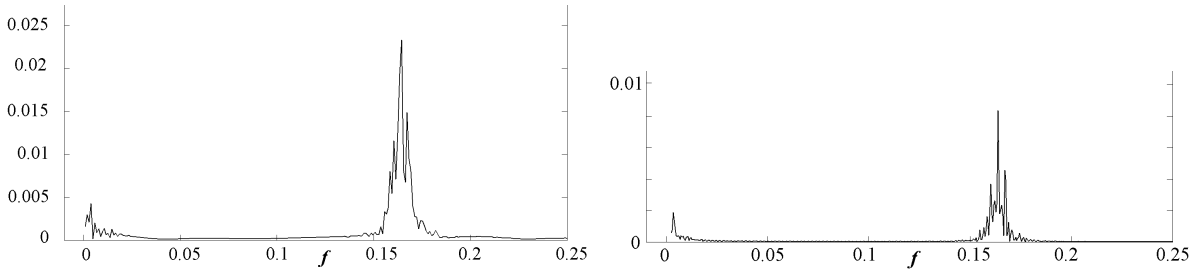

Figure 10: Spectrum for u_x and u_z.

7. Klimontovich Yu. L. (1992), About the necessity and possibility of unified description of kinetical and hydrodynamical processes, *Theoretical and Mathematical Physics*, Vol. 92, pp. 312-330.
8. Streater R.F.(2001), The dissipative continuity equation, 17 th International Conference on Transport Theory, Imperial College, 8 -14 July, 2001.
9. Brenner H. (2006), Fluid Mechanics Revisited, *Physica A*, Vol. 370, pp. 190–224.
10. Ottinger H.C. (2005), Beyond equilibrium thermodynamics Hoboken, John Wiley.
11. Alexeev B.V. (2004), Generalized Boltzmann physical kinetics, Elsevier, Amsterdam.
12. B.F. Armaly, F. Durst, J.C.F. Pereira et al. Experimental and theoretical investigation of backward-facing step flow. *J. of Fluid Mech.* 12:473-496, 1983.
13. H.P. Rani, T.W.H. Sheu: Nonlinear dynamics in a backward-facing step flow Physics of Fluids. **18**, 084101 (2006)
14. C.D. Langhe, B. Merci, E. Dick. Renormalization group based hybrid RANS/LES modeling *ERCOFTAG bulletin*, 72:55-59, 2007.
15. Elizarova T.G., Kalachinskaya I.S., Sheretov Yu.V., Shil'nikov E.V. Simulation of separating flows over a backward-facing step. Computational Mathematics and Modeling, **15**, No. 2, pp.167-193 (2004)